# How the 1999 Climate Shift Has Changed MJO Propagation Diversity

BIN WANG[a] AND TIANYI WANG[a,b]

[a] *Department of Atmospheric Sciences and International Pacific Research Center, University of Hawai'i at Mānoa, Honolulu, Hawaii*
[b] *Marine Science and Technology College, Zhejiang Ocean University, Zhoushan, China*

(Manuscript received 30 September 2022, in final form 29 January 2023)

ABSTRACT: An improved understanding of how the climate mean-state variation modulates MJO property is key to comprehending projected MJO's future change. After 1999, the Pacific shows a mega La Niña–like cooling, enhancing mean precipitation and MJO variability over the Maritime Continent and the northern Indo-Pacific warm pool. However, how the 1999 shift changed MJO propagation has not been studied. This study has detected significant changes in MJO propagation diversity across the 1999 climate shift. From epoch period 1 (P1; 1979–98) to P2 (1999–2018), the number of standing oscillation (SO) events has doubled, but the fast eastward-propagating (fast) events have decreased by 42%, the slow eastward-propagating events have increased by 150%, and the zonal extents of the MJO propagation have shifted westward by 10°–20° of longitude. The SO (fast) events are often associated with a La Niña–like (El Niño–like) mean state. Therefore, the La Niña–like mean-state change associated with the 1999 climate shift has increased the chance for more SO but fewer fast events. The La Niña–like mean-state shift has also promoted the slow-propagating events from the Indian Ocean to the western Pacific (WP) by increasing moisture content, convective instability, low-level convergence, and upward transport moisture over the equatorial WP. The results imply that the future change of the MJO propagation would critically depend on how the anthropogenic forcing changes the Indo-Pacific sea surface temperature pattern, especially an El Niño–like or La Niña–like warming pattern. The existing uncertainties in projecting the Pacific warming pattern could pose a significant ambiguity in anticipating MJO's future change.

KEYWORDS: ENSO; Madden-Julian oscillation; Climate change; Intraseasonal variability; Multidecadal variability; Tropical variability

## 1. Introduction

The Madden–Julian oscillation (MJO) profoundly influences extreme weather events worldwide (Zhang 2013). Changes in MJO behavior under increasing anthropogenic forcing have become a keen societal concern. Climate models project an increase in the MJO amplitude and frequency (Chang et al. 2015; Bui and Maloney 2019) and a faster eastward propagation (Adames et al. 2017; Cui and Li 2019; Rushley et al. 2019; Bui and Maloney 2020) in a warmer climate. However, projected MJO changes in the models are sensitive to sea surface temperature (SST) warming patterns. A zonally symmetric warming decreases MJO precipitation and wind variability, while globally uniform warming significantly increases MJO precipitation amplitude (Maloney and Xie 2013). The MJO circulation is less changed than the convection in the models, due to enhanced static stability that weakens the circulation (Bui and Maloney 2018; Maloney et al. 2019). The key to an accurate projection of future change of MJO is understanding how the climate mean-state change modulates MJO behavior.

Toward the end of the twentieth century, the Pacific Ocean experienced a dramatic change after the strongest 1997/98 El Niño of the twentieth century, known as a climate shift (Lyon et al. 2014). After 1999, the eastern Pacific triangle region cools while the western Pacific (WP) K-shaped region warms (Fig. 1a). This mega La Niña–like SST change (Wang et al. 2013) induced suppressed convection over the equatorial central Pacific and enhanced convection over the Maritime Continent and the northern Indo-Pacific warm pool (Fig. 1b). Correspondingly, the MJO variability during boreal winter, which is measured by the standard deviation of the 20–70-day bandpass-filtered precipitation anomalies, follows the mean-state precipitation change closely (Fig. 1c), suggesting that an increased mean-state convection could induce increased MJO convective activity. However, how the 1999 climate shift has changed MJO propagation is unidentified. The recent four decades' reliable observations provide an excellent opportunity to investigate how MJO propagation has responded to climate mean-state change. The present work attempts to unravel the processes by which the 1999 climate mean-state shift may alter the MJO propagation.

Previous studies of the mean state impacts on MJO have resulted in mixed results. On the interannual time scale, sea surface temperature does not control the global-scale MJO strength (Hendon et al. 1999; Slingo et al. 1999) but significantly affects the MJO intensity on regional scales, especially over the WP (Teng and Wang 2003; Moon et al. 2011; Liu et al. 2016; Suematsu and Miura 2018). On a decadal scale, MJO activity was enhanced in association with the eastern Pacific El Niño development during 1985–2000 (Gushchina and Dewitte 2019). The MJO variance, represented by the power spectra of zonal winds or satellite-derived outgoing longwave radiation and brightness temperature, shows a decreasing trend (Suhas and Goswami 2010; Raghavendra et al. 2019). However, the MJO changes on the multidecadal time scale involve global warming and internal variability, and the precise causes are unknown.

*Corresponding author*: Tianyi Wang, tianyi@hawaii.edu

DOI: 10.1175/JCLI-D-22-0749.1

© 2023 American Meteorological Society. For information regarding reuse of this content and general copyright information, consult the AMS Copyright Policy (www.ametsoc.org/PUBSReuseLicenses).

Brought to you by University of Hawaii at Manoa, Library | Unauthenticated | Downloaded 05/30/23 01:47 AM UTC

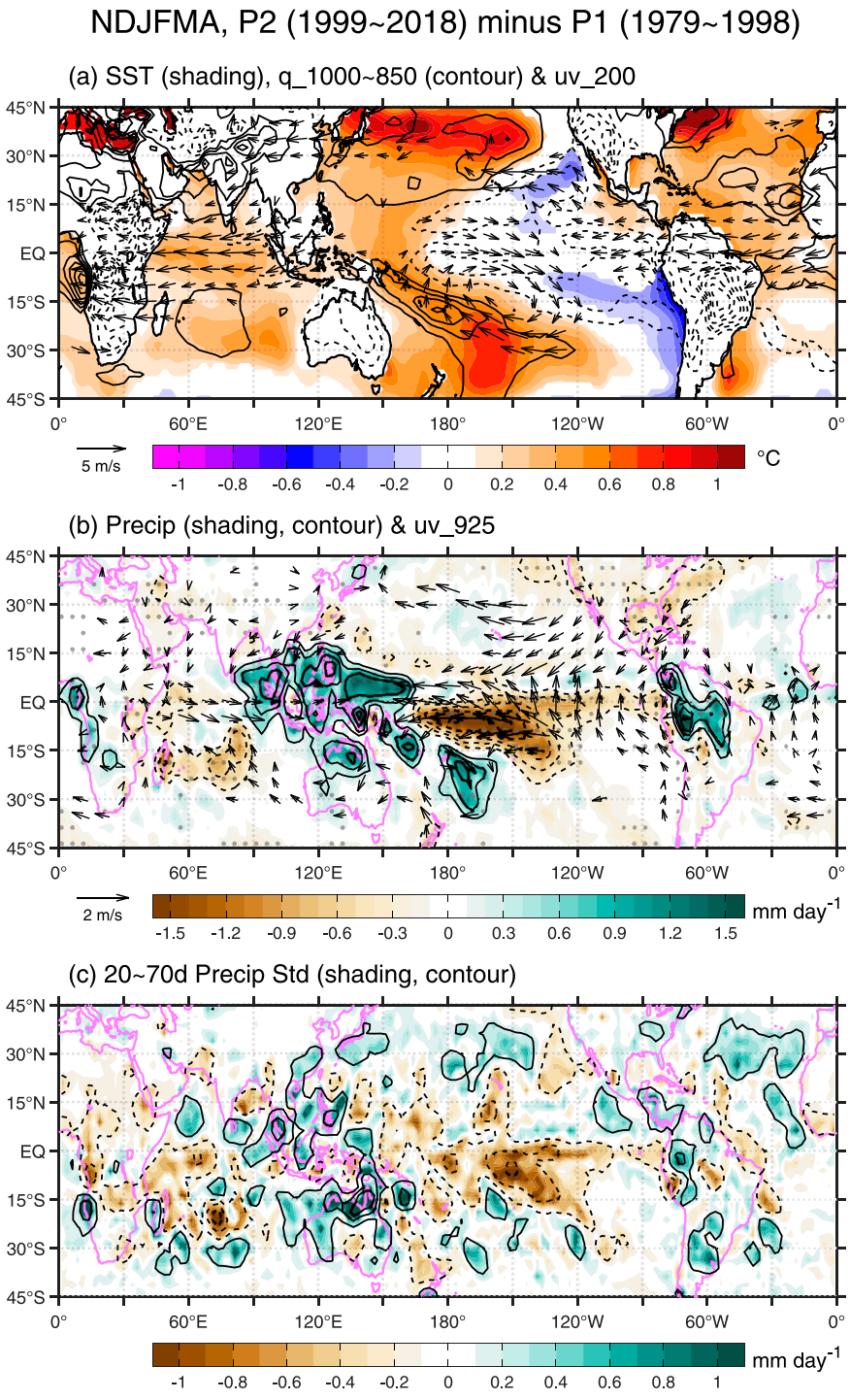


FIG. 1. Boreal winter (NDJFMA) climatological mean-state changes (1999–2018 minus 1979–98). (a) SST (shading; units: °C), 1000–850 hPa integrated specific humidity (contour interval: 0.15 kg $m^{-2}$ with zero omitted, and negative dashed), and 200 hPa winds (vectors). Only wind vectors and SST anomalies with a significance level of 0.05 are shown. (b) CMAP precipitation rate (contour interval: 0.3 mm $day^{-1}$ with zero omitted and negative dashed), and 925 hPa winds (vectors). Only wind vectors with a significance level of 0.05 are shown. Stippling denotes where the shaded values are significant at the 0.05 level. (c) Standard deviations of the 20–70-day CMAP precipitation rate (contour interval: 0.4 mm $day^{-1}$, starts from ±0.2 mm $day^{-1}$ with negative dashed). Significant values at the 0.05 level are shown, estimated by a two-tailed, two-sample *F* test. A three-point running mean was applied to the contours in (b) and (c).

Brought to you by University of Hawaii at Manoa, Library | Unauthenticated | Downloaded 05/30/23 01:47 AM UTC

To explain why the MJO propagation might change, we need to comprehend why the MJO moves eastward in the first place. The MJO's horizontal circulation structure consists of an eastern Kelvin wave and a western Rossby wave component coupled with a convective complex (Rui and Wang 1990). The boundary layer (BL) convergence feedback provides a robust mechanism for the eastward propagation because the MJO convective heating-induced BL convergence is located east of convection (Hendon and Salby 1994; Kiladis et al. 2005). Wang and Rui (1990) have shown that the Kelvin wave–induced BL convergence coincides with the Kelvin wave low and easterly flow, while the Rossby wave–induced BL convergence coincides with not only the Rossby wave lows but also a maximum equatorial convergence to the east of the Rossby wave lows. Therefore, the Kelvin and Rossby waves jointly produce a unified BL moisture convergence to the east of MJO convection. This theoretical result is supported by observations (Maloney and Hartmann 1998; Sperber 2003; Tian et al. 2006; Berrington et al. 2022) and 27 models' simulations (Wang et al. 2018). As a result, the boundary layer convergence gradually deepens the moist boundary layer (Kemball-Cook and Weare 2001) and increases convective instability (Hsu and Li 2012). These preconditioning processes lead to a "stepwise" transition from shallow cumulus and congestus clouds to deep convection and stratiform anvil clouds (Johnson et al. 1999; Del Genio et al. 2012). The BL convergence and associated premoistening, predestabilization, and shallow and congestus clouds all lead the MJO major convection, promoting MJO's eastward movement. The boundary layer moisture convergence, along with the stratiform cloud condensational heating (Lin et al. 2004), is critical in generating a westward- and upward-tilted MJO structure in the specific humidity, equivalent potential temperature, ascending motion, and diabatic heating.

The MJO propagation was found to be intimately related to its vertically tilted structure. By examining 27 general circulation model simulations, Jiang et al. (2015) show that the observed vertical westward tilt with the altitude of the MJO is well simulated in good MJO models but not in poor ones. They found that damped Kelvin wave responses to the east of convection in the lower troposphere could be responsible for the missing MJO preconditioning process in these poor MJO models, suggesting a link between the vertical and horizontal circulation structures. Wang et al. (2018) further show that the models that simulate better three-dimensional dynamic and thermodynamic structures of MJOs generally reproduce better eastward propagations.

The essential dynamics of MJO involve a trio interaction among the convective heating, the equatorial waves and boundary layer dynamics, and the moisture feedback (Wang et al. 2016; Wang and Chen 2017). The trio-interaction theory demonstrates that different parameterization schemes can produce different MJO horizontal circulation patterns, especially the relative strength of the Rossby wave westerly versus Kelvin wave easterly. Faster propagation is associated with relatively intense Kelvin easterly, consistent with the finding from observation and multimodel simulations (Jiang et al. 2015; Wang and Lee 2017; Wang et al. 2018; Berrington et al. 2022). Kim et al. (2016) observed that the Indian Ocean convection anomaly preferentially makes eastward propagation and reaches the western Pacific when the dry anomaly over the eastern Maritime Continent and the western Pacific is stronger, implying a coupling between MJO eastward propagation and the leading suppressed convection. Chen and Wang (2018) pointed out that the leading suppressed convection enhances the coupling of Indian Ocean convection and the Walker cell to its east (front Walker cell) by increasing the zonal heating gradient. The enhanced front Walker cell strengthens the low-level easterly, which increases BL convergence, facilitating MJO eastward propagation.

Kim et al. (2014) used the column-integrated moist static energy (MSE) budget analysis to show that horizontal advection moistens the atmosphere to the east of the positive MSE anomaly, leading to the eastward propagation of the positive MSE anomaly. The MSE budgets were diagnosed, and the zonal asymmetry in MSE tendency can distinguish the propagations between good and poor models (Jiang et al. 2015; Wang et al. 2017). The MSE budget is a kinematic diagnostic tool and cannot offer definitive causal proof of the processes that control MJO phase speed. However, the terms contributing to the MSE tendency can be suggestive of the MJO's dynamics (Wang et al. 2017). Note that the dominant advective processes remain debated. Kim et al. (2016) emphasized the role of the Rossby wave response and associated meridional moisture advection. Wang et al. (2017) find that the zonal asymmetry of upper–midtropospheric vertical velocity anomalies acting on background MSE vertical gradient (vertical advection) is critical. Their numerical experiments show the stratiform heating at the rear of MJO convection is responsible for the zonal asymmetry of vertical velocity anomaly, suggesting the importance of the second-baroclinic-mode vertical velocity. On the other hand, Jiang et al. (2015) found that zonal MSE advection plays the leading role. The discrepancies are possibly due to the dependence of the calculated MSE tendency on the locations chosen for the computation.

This work aims to identify changes in MJO propagation from the pre-1999 (1979–98) to post-1999 (1999–2018) climate-shift epochs and to understand the mechanisms by which the mean state changes the MJO propagation. We detect the change from the perspective of MJO propagation diversity changes. While each MJO event propagates and evolves differently from others, a nonlinear *k*-mean cluster analysis has identified four prototypes of MJO propagation: standing, jumping, slow, and fast eastward propagation (Wang et al. 2019). Here, we hypothesize that the tropical mean-state changes might alter different types of MJO, which offers an opportunity to understand better how the mean-state changes could determine the changes in the MJO propagations. Section 2 describes the data and methodology. Section 3 presents MJO diversity changes by comparing pre-1999 and post-1999 epochs. In section 4, we explore the causes of the MJO diversity change. Section 5 presents conclusions and a discussion.

## 2. Data and method

We used outgoing longwave radiation (OLR) to depict the deep convection associated with MJO. The daily OLR data

Brought to you by University of Hawaii at Manoa, Library | Unauthenticated | Downloaded 05/30/23 01:47 AM UTC

were interpolated by the National Centers for Environmental Prediction and National Oceanic and Atmospheric Administration (Liebmann and Smith 1996). The CPC Merged Analysis of Precipitation (CMAP) (Xie and Arkin 1997) data were also adopted to complement OLR. For atmospheric circulation, we used daily averaged winds, temperature, and specific humidity from 1000 to 100 hPa derived from the latest European Centre for Medium-Range Weather Forecasts Reanalysis (ERA5) (Hersbach et al. 2020). To study the background SST conditions, we adopted the SST dataset from the NOAA Extended Reconstructed Sea Surface Temperature (ERSST), version 5 (Huang et al. 2017). All the datasets covered the 40 years from 1979 to 2018 and were interpolated to the same 2.5° × 2.5° grid as the OLR data.

The climatological annual cycle consists of the annual mean and the first three Fourier harmonics of the climatological daily mean time series. Daily anomalies are the departure from the climatological annual cycle. We applied a 20–70-day bandpass filter to obtain the MJO signals. The analysis focuses on boreal winter from 1 November to 30 April (NDJFMA).

Following Waliser et al. (2009), we depict MJO eastward propagation by a lag–longitude correlation map (also known as the Hovmöller diagram) of OLR anomalies along the equator between 10°S and 10°N. An MJO event was selected if the box-averaged OLR over the reference location (10°S–10°N, 75°–95°E) is below one standard deviation for five successive days. This reference location displays the maximum MJO variance during boreal winter. The reference date (day 0) for a selected MJO event was chosen as the day when the averaged OLR in the reference location reached its minimum.

Following Wang et al. (2019), we applied the *k*-means cluster analysis with correlation as the distance metric (Kaufman and Rousseeuw 2009) to objectively classify diverse MJO propagation patterns along the equator for all selected events. For each qualified MJO event, the cluster analysis domain in the Hovmöller diagram covers 30 days from days −10 to 20 and a longitudinal extent from 60°E to 180°. A zonal three-point running mean was applied to the Hovmöller diagram to remove small-scale noises. The analysis focused only on the MJO wet phase. For the *k*-means cluster analysis, the regions where OLR anomalies are higher than $-5$ W m$^{-2}$ are set to zero. The *k*-means clustering was repeated 5000 times to obtain the best results. We used the silhouette clustering evaluation criterion to assess the skill of cluster analysis. The silhouette value, ranging from −1 to +1, judges how similar a member fits its cluster compared to others. A higher silhouette value implies that the member is well matched to its cluster and poorly matched to neighboring clusters.

There are 117 selected cases during the 40 years from 1979 to 2018. To detect the decadal variation of MJO, we examine two 20-yr periods: Period 1 (P1) covers the boreal winter from 1979/80 to 1998/99, and period 2 (P2) covers the winter from 1999/2000 to 2018/19. Cases with a silhouette value lower than 0.02 were excluded from the corresponding clusters, as they were considered sufficiently "dissimilar" to the corresponding centroid of the cluster. By removing 11 dissimilar cases, 106 events were used to perform composite analyses.

In the composite Hovmöller diagrams of propagating MJOs, a line indicates the phase propagation of main MJO convection anomalies (OLR $< -5$ W m$^{-2}$) is first identified based on minimizing the total OLR anomalies integrated along the line. The phase speed is then computed from the slope of the line.

## 3. MJO diversity and its changes from pre-1999 to post-1999 epochs

### *a. Standard features of the MJO propagation diversity*

The total of 106 events during the 40 years (1979–2018) consists of 47 events during P1 and 59 events during P2. The events during each epoch were optimally fit into four clusters. Their composite evolutions are shown in Fig. 2. The four clusters for each period have similar common features, suggesting the MJO diversity (types) remain robust, although the total number of significant MJO events has increased by about 25%.

Type I features a quasi-stationary oscillation in the equatorial eastern Indian Ocean (EIO; 10°S–10°N, 70°–90°E). There is a weak sign of origination from 50° to 60°E but no eastward propagation between 70° and 100°E. These cases may be considered nonpropagating MJO events discussed in the literature (e.g., Kim et al. 2014; Feng et al. 2015; DeMott et al. 2018). We name it a regional Standing Oscillation (SO), acknowledging that many purely standing cases are not qualified as MJO events. Type II displays a stationary wet anomaly in the EIO followed by the occurrence of an independent, equatorial, western Pacific convective anomaly. These were named "jump" events by Wang et al. (2019). Types III and IV represent continuous eastward propagation across the Maritime Continent (MC) without notably changing its propagation speed. They are not significantly affected by the "MC barrier" (Zhang and Ling 2017) except for a temporal decrease in the OLR anomaly over the MC due to increased land-fraction and topographic effects over the MC (Hsu and Lee 2005; Inness and Slingo 2006; Wu and Hsu 2009). Types III and IV differ by their propagation speed and zonal extent. Type III propagates slower (3.9 vs 4.8 m s$^{-1}$), while type IV moves faster (5.8 vs 6.8 m s$^{-1}$), so we name types III and IV as Slow and Fast groups, respectively. The fast-moving events extend to 160°W, and the propagation track is about 20° of longitude longer than that of the slow movers.

To what extent does the MC barrier influence the boreal winter MJO? Table 1 summarizes the numbers and percentages of occurrences for each type during the two epochs. For the entire 40-yr period, the SO, jump, slow, and fast events account for about 20%, 22%, 30%, and 28%, respectively. Thus, the eastward-propagating MJO events account for about 58% of the total events. Considering that both SO and jump events are affected by the MC's barrier effect, the MC influenced 19 events (~40%) in P1 and 25 (~42%) events in P2.

### *b. Significant changes in the MJO diversity from pre- to post-1999 periods*

Notable differences exist between the two epochs, suggesting a change in the MJO diversity associated with the 1999 climate shift (Table 1). First, the changes are prominent in the

Brought to you by University of Hawaii at Manoa, Library | Unauthenticated | Downloaded 05/30/23 01:47 AM UTC

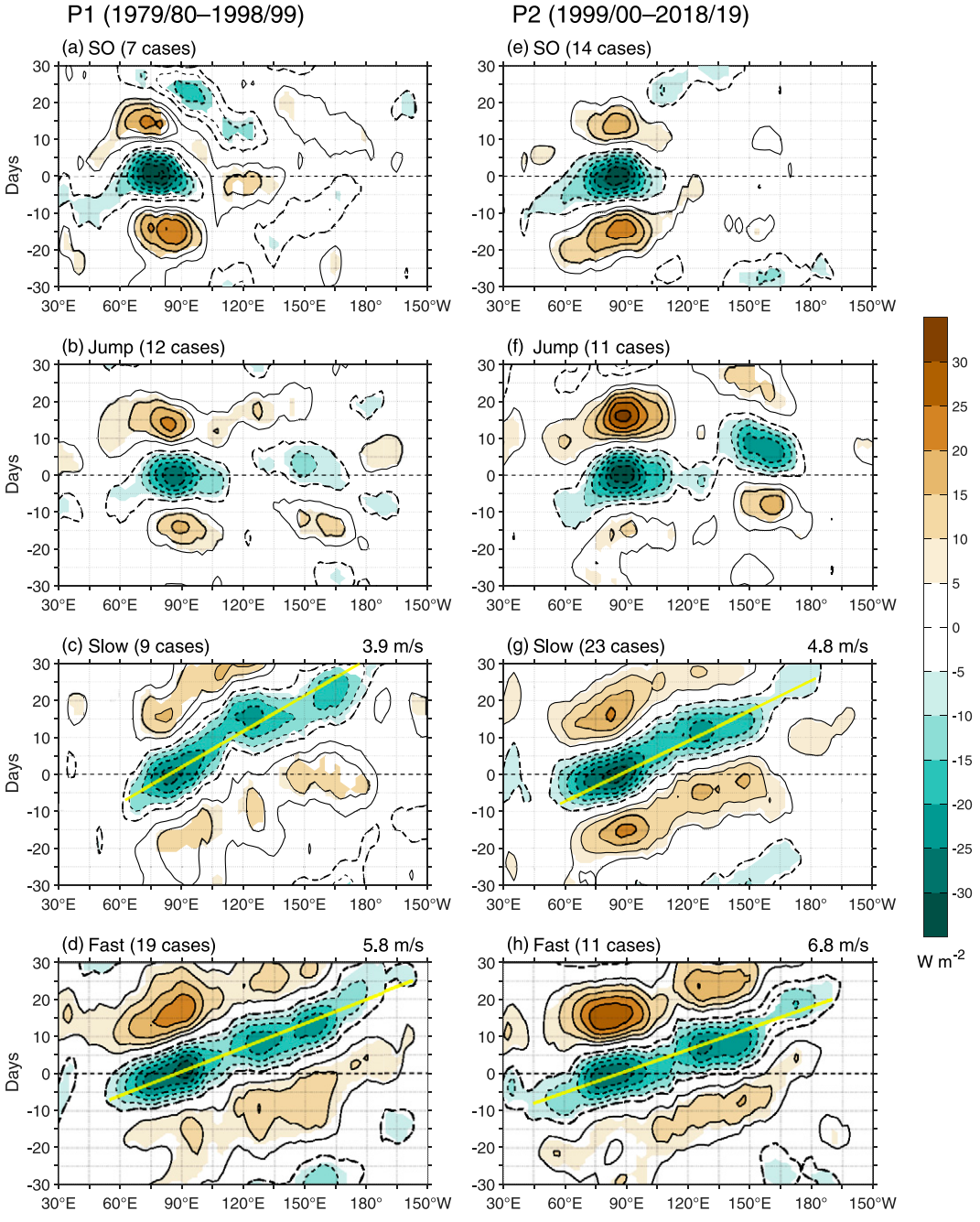


FIG. 2. Four types of MJO propagation patterns along the equatorial belt (10°S–10°N) during (left) P1 (1979–98) and (right) P2 (1999–2018). Shown are composited longitude–time diagrams of 20–70-day OLR anomalies (contours; W $m^{-2}$) averaged between 10°S and 10°N during boreal winter from November to April. The four types of MJO are (from top to bottom): SO, Jump, Slow, and Fast, respectively. The contour interval is 5 W $m^{-2}$, with zero omitted and negative values dashed. The thick dashed contour is $-5$ W $m^{-2}$. The color shading denotes a significance level of 0.05 using a two-tailed Student's *t* test. The solid yellow lines in Slow and Fast types indicate phase propagation of main MJO convection anomalies (OLR $< -5$ W $m^{-2}$), and the estimated phase speed is shown in the top-right corner of the panels.

frequencies of the SO and propagation events. The SO frequency increased from 7 in P1 to 14 in P2. Meanwhile, the eastward propagation types also changed: The slow events increased from 9 in P1 to 23 in P2, but the fast events decreased from 19 in P1 to 11 in P2. The changes in the frequency among different types of MJO events from the pre-1999 to post-1999 epoch are statistically significant by the $\chi^2$ test in the contingency table ($p = 0.02$; Table 1). Second, the

Brought to you by University of Hawaii at Manoa, Library | Unauthenticated | Downloaded 05/30/23 01:47 AM UTC

TABLE 1. The number of occurrences for each type of MJO event during pre-1999 and post-1999 epochs and their corresponding percentages. A $\chi^2$ test on the contingency table (number of occurrences in the first two rows) obtains a $\chi^2$ value of 9.40 with 3 degrees of freedom (DOF), and the corresponding $p$ value is 0.024. Without the Jump column, the $\chi^2$ value of the contingency table is 8.77 and $p = 0.0125$ with 2 DOF.

| Type | SO | Jump | Slow | Fast | Total |
|---|---|---|---|---|---|
| Pre-1999 (1979–98) | 7 (14.9%) | 12 (25.5%) | 9 (19.2%) | 19 (40.4%) | 47 |
| Post-1999 (1999–2018) | 14 (23.7%) | 11 (18.6%) | 23 (39.0%) | 11 (18.6%) | 59 |
| Total | 21 (19.8%) | 23 (21.7%) | 32 (30.2%) | 30 (28.3%) | 106 |

originations of the slow and fast propagations have shifted westward by about 10° of longitude over the Indian Ocean (IO) (Figs. 2c,d,g,h). Their propagations tend to reach about the same longitude at the date line for slow and 165°W for the fast, implying an increased zonal extent from P1 to P2 due to earlier development of the MJO convection in the western equatorial Indian Ocean. Besides, the jump composites show a stronger convective anomaly in the WP during P2.

### c. *Distinct dynamic structures of the different MJO flavors*

Here, we compare the equatorial vertical structure changes among the four types of MJO to obtain clues for the changing propagation characteristics (Fig. 3). The equivalent potential temperature (EPT; contours) represents MSE. The EPT maximum couples the updraft center where MJO major precipitation heating (color shading in Fig. 3) is located. There are common features between P1 and P2. The nonpropagating (SO and jump) events feature a local vertical ascent and MSE structure (Figs. 3a,b). In contrast, the eastward propagation events are characterized by a vertical tilt of updraft and MSE in the lower troposphere, with intense easterlies ahead of the MJO convection (Figs. 3c,d). The differences between the nonpropagating (SO and jump) and propagating (fast and slow) events suggest a robust Kelvin wave easterly, and its coupling to the rearward tilt of the major convective updraft distinguishes MJO eastward propagation from nonpropagating events. This zonal asymmetric structure concurs with the results obtained from observations and multimodel numerical simulations (Jiang et al. 2015; Wang and Lee 2017; Wang et al. 2018; Berrington et al. 2022), as well as theoretical model predictions (Wang et al. 2016; Chen and Wang 2018).

What determines the MJO's eastward propagation speed? The faster eastward propagation displays intense Kelvin wave easterlies from 110°E to 160°W (Figs. 3d,h), while the intense easterlies in the slower propagations tend to be confined to the west of the date line (Figs. 3c,g), suggesting that the eastward propagation speed may intrinsically link to the east–west asymmetry in the zonal wind anomalies as predicted by the convection–dynamics–moisture interaction (trio-interaction) theory (Wang et al. 2016). In addition, the fast propagation events extend high MSE more eastward (over 140°E–180°) than the slow propagation events (Figs. 3d,h versus Figs. 3c,g), indicating an increased boundary layer moisture and convective instability over the equatorial WP (Fig. 3). This feature agrees well with the eastward extension of specific humidity and diabatic heating for the fast propagation documented and demonstrated by Chen and Wang (2020). The two nonpropagating types also differentiate.

In addition to the above common features, the equatorial vertical structures of different types of MJO show subtle differences between the P1 and P2. The vertical structures of the slow events differ between P1 and P2. During P2, the salient cooling and downdraft in the WP (120°–150°E) tightly couples with the MJO updraft (Fig. 3g), resulting in a more significant, rearward-tilted MSE in the lower troposphere and a more systematic, slow eastward propagation from the IO to the WP (Fig. 2g). In contrast, the loose coupling in P1 leads to a "jump-like" slow eastward propagation from the IO to the WP (Fig. 2c). This difference suggests the effects of the enhanced front Walker cell in the MJO's eastward propagation (Chen and Wang 2018). The vertical structures of the jump events also differ between P1 and P2, mainly in the WP. The stronger ascent in the WP during P2 (Fig. 3f) yields a more robust wet-anomaly development (Fig. 2f).

In summary, the four types of MJO exhibit distinct vertical structures along the equatorial belt, providing identifiable precursors to predict the MJO evolution in the next 20 days (Abhik et al. 2023; Xiang et al. 2022). The coherent dynamic and thermodynamic structures among the four types of MJO propagation correspond to distinct propagation characteristics, suggesting a propagation–structure nexus.

## 4. Possible causes of the MJO diversity changes

The MJO has prominent seasonality, indicating that the annual variation of the background mean state remarkably changes the MJO propagation from northern winter to summer (Wang and Xie 1997). The multidecadal variation in the background conditions could affect the MJO propagation. However, the amplitude of the multidecadal variation is substantially smaller than that of the annual variation. Is the change in the mean state from the pre-1999 to post-1999 period large enough to modify MJO behavior? If so, how does the mean-state change alter the MJO propagation?

Let us first examine the mean-state change related to the climate regime shift toward the end of the twentieth century. Figure 4 shows that the equatorial Indo-Pacific mean state averaged between 10°S and 10°N has experienced notable changes during the NDJFMA season. SST has increased over the IO and western Pacific (30°E–180°) with maximum warming of 0.4°C near 150°E, whereas it decreased over the eastern Pacific by about −0.2°C (Fig. 4c). Following the SST change, the specific humidity and equivalent potential temperature or MSE have increased significantly over the eastern IO and WP

Brought to you by University of Hawaii at Manoa, Library | Unauthenticated | Downloaded 05/30/23 01:47 AM UTC

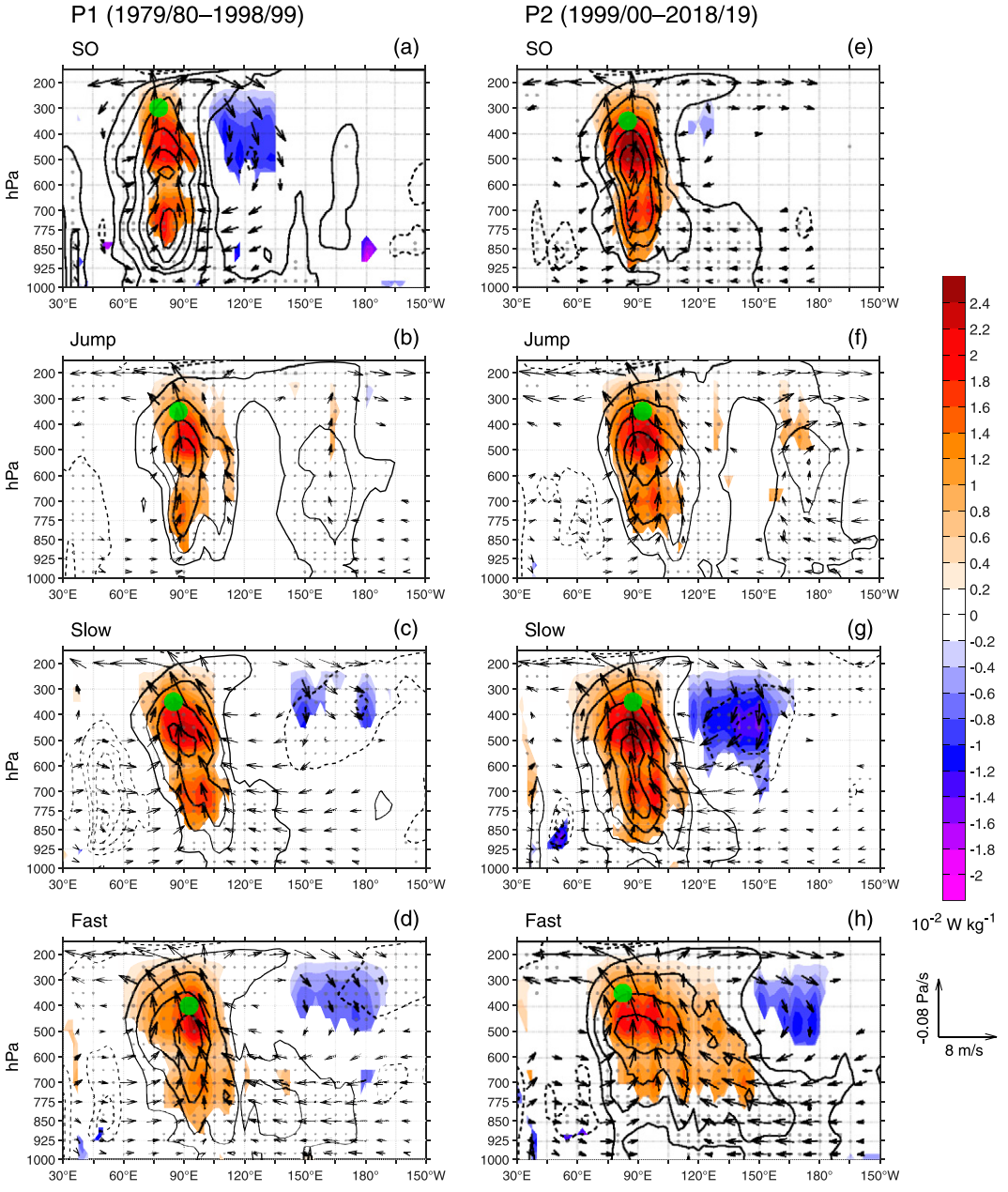


FIG. 3. Zonal–vertical structures of the four types of MJO along the equatorial belt (10°S–10°N) during (left) P1 (1979–98) and (right) P2 (1999–2018). Shown are composited circulation (vectors), EPT (contour interval: 0.5 K, with zero omitted and negative values dashed), and precipitation heating (color shading; in units of $10^{-2}$ J kg$^{-1}$ s$^{-1}$) anomalies. Rows show (from top to bottom) SO, Jump, Slow, and Fast, respectively. Vectors represent the zonal and vertical velocities (units are m s$^{-1}$ for zonal wind and 0.01 Pa s$^{-1}$ for vertical pressure velocity). Only wind vectors and precipitation heating anomalies with a significance level of 0.05 are shown. Stippling denotes where the EPT anomalies are significant at the 0.05 level. The green circle indicates the location of maximum upward motion.

(60°–160°E) with the maximum over the MC (120°–150°E) (Fig. 4a). Correspondingly, the convective instability measured by the 700 hPa minus 400 hPa EPT increased from 90° to 170°E by about 2 K (Fig. 4b). The increased westward SST gradients strengthen easterly trade winds, enhancing boundary layer wind convergence over the eastern MC and WP with the maximum convergence of $6 \times 10^{-7}$ s$^{-1}$ at 150°E (Fig. 4b), leading to enhanced mean upward motion there. The increased convective heating produces easterly vertical wind shear (upper-level easterly and low-level westerly) to the west of 150°E over the IO and MC (60°–130°E) and westerly vertical shear east of 150°E over the central-eastern Pacific (Fig. 4a). In

Brought to you by University of Hawaii at Manoa, Library | Unauthenticated | Downloaded 05/30/23 01:47 AM UTC

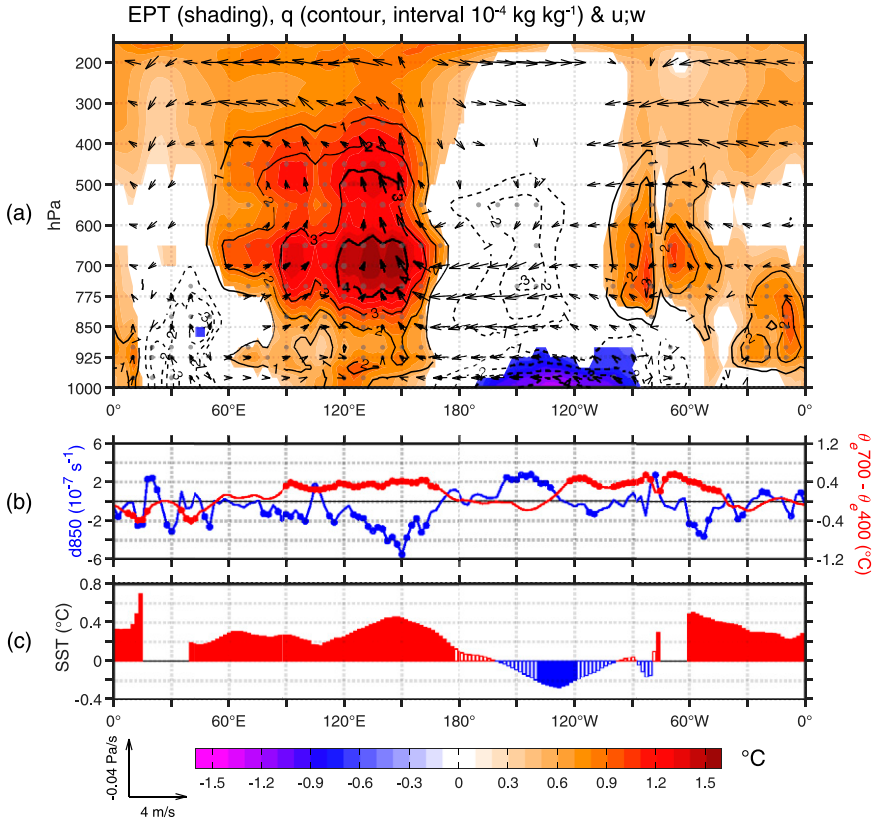


FIG. 4. Boreal winter (NDJFMA) climatological mean-state changes (1999–2018 minus 1979–98): (a) longitudinal–height diagram along the equatorial belt averaged between 10°S and 10°N for EPT (shading; units: °C), specific humidity (contour interval: $10^{-4}$ kg kg$^{-1}$ with zero omitted), and zonal–vertical circulation (vectors); (b) 850 hPa divergence (blue) and convective instability index ($\theta_{e700} - \theta_{e400}$; red); (c) SST. Only wind vectors and shading with a significance level of 0.05 are shown. For one-dimensional plots, the anomalies with a significance level of 0.05 are marked by a circle or shown as solid bars.

summary, the mean-state thermodynamic and dynamic conditions have changed. Changes in thermodynamic conditions include increased moisture content, moist static energy, and convective instability over the Indo-Pacific warm pool. Dynamic condition changes include subsidence over the eastern Pacific and ascending motion over the warm pool. These atmospheric circulation changes are driven by tropical SST changes.

Why do SO events substantially increase while the fast eastward-propagating events decrease sharply from P1 to P2? To address this question, we examined the SST anomalies associated with these two types of MJO events (Fig. 5). The SO events are often associated with a significant sea surface cooling over the central Pacific, resembling a La Niña state (Fig. 5a). The mean-state change from P1 to P2 resembles a La Niña–like change (Figs. 1b and 4). This mean-state change may favor more SO events. During P1, five La Niña years took place during the northern winters of 1983/84, 1984/85, 1988/89, 1995/96, and 1998/99. Nevertheless, during P2, eight La Niña winters occurred, including 1999/2000, 2000/01, 2005/06, 2007/08, 2008/09, 2010/11, 2011/12, 2016/17, and 2017/18 [according to Climate Prediction Center Oceanic Niño Index (ONI; noaa.gov)]. More-frequent La Niña winters would increase the likelihood of SO events. This might explain why the SO events doubled from the pre-1999 (P1) to post-1999 (P2) epochs.

On the other hand, the fast eastward-propagating events tend to take place when the central Pacific is abnormally warm, reminiscent of El Niño (Fig. 5b). When the central-eastern Pacific warms, the Indo-Pacific warm pool and the associated active convective region expand eastward, which favors enlarging the zonal extent of the MJO easterlies because active MJO events occur over the warm ocean (Zhang 2005). The observed wavenumber–frequency power spectrum of MJO signals (Wheeler and Kiladis 1999) and the theoretical studies (Adames and Kim 2016; Fuchs and Raymond 2017; Chen and Wang 2019) have shown that the MJO propagation speed is proportional to its zonal scale. The La Niña cooling has the opposite effect, reducing the MJO's zonal extent. Thus, the La Niña–like mean-state change from P1 to P2 does not favor fast events. Therefore, the mean-state change from P1 to P2 could be responsible for reducing the fast-propagating events from P1 to P2.

Brought to you by University of Hawaii at Manoa, Library | Unauthenticated | Downloaded 05/30/23 01:47 AM UTC

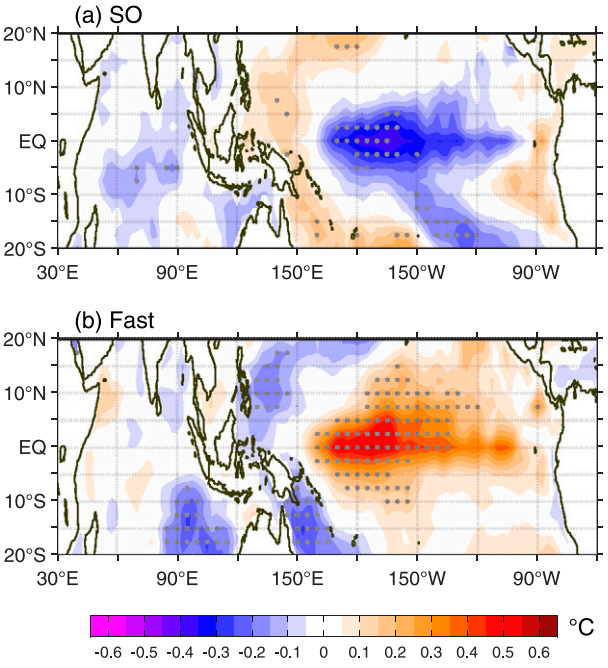


FIG. 5. Composite background SST anomalies associated with the (a) SO and (b) Fast types of MJO events during 1979–2018. The background SST anomalies for each type of MJO event are composited the 3-month average of SST anomalies, with the central month being the month that contains day 0 of an MJO event. Stippling denotes significant signals at the 0.05 level.

Results in Fig. 2 indicate that the MJO initiation in P2 tends to be more active over the western equatorial Indian Ocean, while the strong MJO convective anomalies ($<-15$ W m$^{-2}$) tend to be confined west of 150°E over the WP. The MJO propagation track also has a westward shift. We argue that the central-eastern Pacific cooling during P2 generates subsidence in the central Pacific (Fig. 4), prohibiting MJO's strong convection from extending eastward into the central or eastern Pacific. Meanwhile, it enhances upward motion over the Indian Ocean and increases moisture due to warmer SST (Fig. 4), promoting its initiation in the IO.

Finally, the slow-propagating events were more than doubled from P1 to P2, and the jump events have a stronger wet anomaly over the WP (Fig. 2). These changes are arguably related to the background changes over the Indo-Pacific warm pool. During P2, the high moisture content and convective instability over the equatorial WP (Fig. 4) promote the development of the MJO convective anomaly, enhancing the WP convective anomalies in the jump events. The mean-state low-level convergence can strengthen upward transport moisture and moisten the midtroposphere, conducive to shallow and congestus cloud development east of the MJO convection. The enhanced background convection over the WP during P2 also makes it more sensitive to an anomalous descent through positive circulation–convection feedback (Wang and Li 2021), causing a more potent front Walker cell effect depicted by a greater downdraft and cooling to the east of the MJO upward motion (Fig. 3). These conditions arguably promote the slow-propagating events to the WP. Why do these changes favor slow events rather than fast events? MJO propagation is slower when the effective static stability reduces (Wang 1988). Effective static stability is the dry static stability reduced by diabatic heating. During P2, the mean precipitation increases from 90° to 160°E (Fig. 1b), implying an enhanced background diabatic heating or a reduced effective static stability. Therefore, the slow eastward-propagating event is favored. Another reason is that an El Niño–like mean state facilitates fast propagation (Fig. 5b). However, during P2, the mean-state SST shows a La Niña–like change (Fig. 1a), which does not favor fast propagation.

Other factors can also change MJO propagation. The increase in the background humidity over the WP (Fig. 4) can promote eastward propagation because an MJO easterly can transport more moisture westward to create a positive MSE tendency to the east of the MJO. The increased easterly vertical wind shear over the IO (Fig. 4) would enhance the Rossby wave response (Wang and Li 2021), strengthening dry MSE advection to the west of the MJO convection, generating an eastward MSE tendency and favoring eastward propagation (Sobel et al. 2014).

## 5. Conclusions and discussion

We have detected changes in MJO propagation diversity from the pre-1999 (P1) to post-1999 (P2) climate shift. The main findings are highlighted as follows:

- The four types of MJO events, named Standing Oscillation (SO), jump over the Maritime Continent (jump), slow eastward propagation (slow), and fast eastward propagation (fast), remain robust from P1 to P2 (Fig. 2). However, the total numbers of significant MJO events have increased by about 25%.
- We detected significant changes in MJO propagations across the 1999 climate shift (Fig. 2, Table 1). From P1 to P2, the SO frequency has doubled, and the slow-propagating events have increased by 150%; meanwhile, the fast-eastward-propagating events have decreased by 42%. Second, the zonal extents of the eastward propagation have shifted westward by about 10°–20° of longitude due to MJO initiation in the western Indian Ocean. The jump events exhibit more active convection over the WP (Fig. 2).
- The La Niña–like mean-state-change-associated 1999 climate shift (Figs. 1 and 4), with more frequent La Niña episodes, increases the chance for more SO but fewer fast propagation events. This is because the SO events are often associated with a La Niña state, whereas the fast propagation events occur preferably in an El Niño–like mean state (Fig. 5).
- The La Niña–like mean-state shift from P1 to P2 has increased moisture content and convective instability, and low-level convergence and upward transport of moisture over the equatorial WP (Fig. 3). These favorable thermodynamic and dynamic conditions may promote the slow-propagating events from the IO to the WP and enhance the WP convective anomalies in the jump events. The associated

Brought to you by University of Hawaii at Manoa, Library | Unauthenticated | Downloaded 05/30/23 01:47 AM UTC

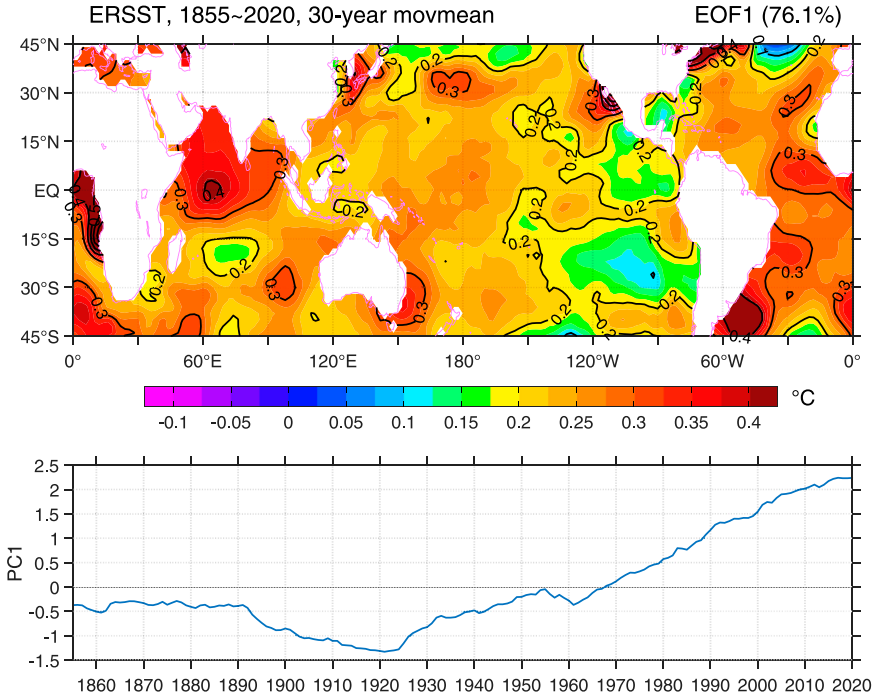


FIG. 6. (top) The leading empirical orthogonal functions (EOFs) pattern (contour interval: 0.1°C) and (bottom) the corresponding principal component 30-yr running-mean SST during NDJFMA from 1855 to 2020. The region for EOF analysis is 30°S–30°N, 30°E–60°W.

opposite mean-state change over the equatorial central-eastern Pacific hinders the propagating events and causes a westward shift of the propagation tracks.

A warmer Indo-Pacific warm pool during P2 may increase MJO convective variance or intensity in the Indo-Pacific warm pool (Fig. 1c). However, the MJO variance decreases in the central Pacific. As a result, the total MJO convective variance averaged over the tropics was unchanged. On the other hand, the total number of significant MJO events has increased by about 25% from P1 to P2 (Table 1), suggesting that a warmer Indo-Pacific warm pool with improved thermodynamic conditions can stimulate more significant MJO events. Cooling over the eastern Pacific hinders the MJO propagation into the central Pacific but promotes the MJO initiations in the western Indian Ocean.

MJO originated from the EIO and sometimes vanished over the MC (Zhang and Ling 2017). MC's barrier effect on the eastward propagation of the boreal winter MJO was generally recognized (Wang and Rui 1990; Hendon and Salby 1994; Kim et al. 2014; Kerns and Chen 2016; Zhang and Han 2020). The MC barrier effects typically lead to the MJO "prediction barrier" (Inness et al. 2003; Fu et al. 2013; Jiang et al. 2015; Kim et al. 2016). Teleconnection of the MJO usually becomes the strongest when its convection center reaches the eastern edge of the MC (Adames and Wallace 2014). Therefore, it is a keen concern whether this MC barrier effect has experienced decadal variations. Our work shows that during P1 and P2, the slow and fast propagation events account for about 59.6% and 57.6%, respectively. The slight decrease is not statistically significant. The MC barrier effect does not seem to be affected by the climate shift.

The global warming pattern during the historical period from 1855 to 2020, derived from the 30-yr running mean NDJFMA SST (Fig. 6), shows a warmer Indo-Pacific warm pool, but the equatorial eastern Pacific shows slightly weaker warming, suggesting a weak La Niña–like tropical warming. This La Niña–like "trend" pattern is much weaker than the La Niña–like 1999 climate shift pattern (Fig. 1). Therefore, we argue that the 1999 climate shift might broadly reflect a multidecadal internal variation. The observed trend pattern from 1855 to 2020 might be too insignificant to change MJO propagation diversity.

The results obtained from analysis of the present-day change of the MJO suggest that the correct projection of the future SST pattern in the tropical Indo-Pacific Ocean is key to predicting the MJO change. The present work stresses the crucial role of the changes in the Pacific east–west SST gradients on MJO propagation. Unfortunately, future mean-state SST changes projected by the climate models have remained uncertain due to the models' biases in simulated mean state in the current climate (e.g., Seager et al. 2019). This uncertainty could pose a significant ambiguity in anticipating the future change of MJO.

The correlation metric used for measuring the distance in the cluster analysis is adequate for detecting propagation but cannot reveal the amplitude evolution. However, our sensitivity test shows that using the Euclidean distance metric might be suitable for detecting intensity evolution but could undermine

Brought to you by University of Hawaii at Manoa, Library | Unauthenticated | Downloaded 05/30/23 01:47 AM UTC

propagation signals. The current cluster analysis is one-dimensional along the equator only. More sensitivity studies are requested to examine 2D propagation patterns and the dependence of the propagation diversity on the chosen reference points.

*Acknowledgments.* The authors acknowledge the support by NSF/Climate Dynamics Award 2025057. This is SOEST Contribution Number 11654, IPRC Contribution Number 1597, and ESMC Number 404.

*Data availability statement.* The OLR and CMAP data are provided by the NOAA/OAR/ESRL PSL, Boulder, Colorado, from their Web site at https://psl.noaa.gov/. The ERA5 dataset is available at Copernicus Climate Change Service Climate Data Store (CDS) at https://cds.climate.copernicus.eu/#!/search?text=ERA5&type=dataset. The ERSST data are available at https://www.ncei.noaa.gov/products/extended-reconstructed-sst.

## REFERENCES

Abhik, S., H. H. Hendon, and C. Zhang, 2023: The Indo-Pacific Maritime Continent barrier effect on MJO prediction. *J. Climate*, **36**, 945–957, https://doi.org/10.1175/JCLI-D-22-0010.1.

Adames, Á. F., and J. M. Wallace, 2014: Three-dimensional structure and evolution of the vertical velocity and divergence fields in the MJO. *J. Atmos. Sci.*, **71**, 4661–4681, https://doi.org/10.1175/JAS-D-14-0091.1.

——, and D. Kim, 2016: The MJO as a dispersive, convectively coupled moisture wave: Theory and observations. *J. Atmos. Sci.*, **73**, 913–941, https://doi.org/10.1175/JAS-D-15-0170.1.

——, ——, A. H. Sobel, A. Del Genio, and J. Wu, 2017: Changes in the structure and propagation of the MJO with increasing $CO_2$. *J. Adv. Model. Earth Syst.*, **9**, 1251–1268, https://doi.org/10.1002/2017MS000913.

Berrington, A. H., N. Sakaeda, J. Dias, and G. N. Kiladis, 2022: Relationships between the eastward propagation of the Madden-Julian oscillation and its circulation structure. *J. Geophys. Res. Atmos.*, **127**, e2021JD035806, https://doi.org/10.1029/2021JD035806.

Bui, H. X., and E. D. Maloney, 2018: Changes in Madden-Julian oscillation precipitation and wind variance under global warming. *Geophys. Res. Lett.*, **45**, 7148–7155, https://doi.org/10.1029/2018GL078504.

——, and ——, 2019: Mechanisms for global warming impacts on Madden–Julian oscillation precipitation amplitude. *J. Climate*, **32**, 6961–6975, https://doi.org/10.1175/JCLI-D-19-0051.1.

——, and ——, 2020: Changes to the Madden-Julian Oscillation in coupled and uncoupled aquaplanet simulations with $4xCO_2$. *J. Adv. Modeling Earth Syst.*, **12**, e2020MS002179, https://doi.org/10.1029/2020MS002179.

Chang, C.-W. J., W.-L. Tseng, H.-H. Hsu, N. Keenlyside, and B.-J. Tsuang, 2015: The Madden-Julian Oscillation in a warmer world. *Geophys. Res. Lett.*, **42**, 6034–6042, https://doi.org/10.1002/2015GL065095.

Chen, G., and B. Wang, 2018: Effects of enhanced front Walker cell on the eastward propagation of the MJO. *J. Climate*, **31**, 7719–7738, https://doi.org/10.1175/JCLI-D-17-0383.1.

——, and ——, 2019: Dynamic moisture mode versus moisture mode in MJO dynamics: Importance of the wave feedback and boundary layer convergence feedback. *Climate Dyn.*, **52**, 5127–5143, https://doi.org/10.1007/s00382-018-4433-7.

——, and ——, 2020: Circulation factors determining the propagation speed of the Madden–Julian oscillation. *J. Climate*, **33**, 3367–3380, https://doi.org/10.1175/JCLI-D-19-0661.1.

Cui, J., and T. Li, 2019: Changes of MJO propagation characteristics under global warming. *Climate Dyn.*, **53**, 5311–5327, https://doi.org/10.1007/s00382-019-04864-4.

Del Genio, A. D., Y. Chen, D. Kim, and M.-S. Yao, 2012: The MJO transition from shallow to deep convection in *CloudSat*/CALIPSO data and GISS GCM simulations. *J. Climate*, **25**, 3755–3770, https://doi.org/10.1175/JCLI-D-11-00384.1.

DeMott, C. A., B. O. Wolding, E. D. Maloney, and D. A. Randall, 2018: Atmospheric mechanisms for MJO decay over the Maritime Continent. *J. Geophys. Res. Atmos.*, **123**, 5188–5204, https://doi.org/10.1029/2017JD026979.

Feng, J., T. Li, and W. Zhu, 2015: Propagating and nonpropagating MJO events over Maritime Continent. *J. Climate*, **28**, 8430–8449, https://doi.org/10.1175/JCLI-D-15-0085.1.

Fu, X., J.-Y. Lee, P.-C. Hsu, H. Taniguchi, B. Wang, W. Wang, and S. Weaver, 2013: Multi-model MJO forecasting during DYNAMO/CINDY period. *Climate Dyn.*, **41**, 1067–1081, https://doi.org/10.1007/s00382-013-1859-9.

Fuchs, Ž., and D. J. Raymond, 2017: A simple model of intraseasonal oscillations. *J. Adv. Model. Earth Syst.*, **9**, 1195–1211, https://doi.org/10.1002/2017MS000963.

Gushchina, D., and B. Dewitte, 2019: Decadal modulation of the relationship between intraseasonal tropical variability and ENSO. *Climate Dyn.*, **52**, 2091–2103, https://doi.org/10.1007/s00382-018-4235-y.

Hendon, H. H., and M. L. Salby, 1994: The life cycle of the Madden–Julian oscillation. *J. Atmos. Sci.*, **51**, 2225–2237, https://doi.org/10.1175/1520-0469(1994)051<2225:TLCOTM>2.0.CO;2.

——, C. Zhang, and J. D. Glick, 1999: Interannual variation of the Madden–Julian oscillation during austral summer. *J. Climate*, **12**, 2538–2550, https://doi.org/10.1175/1520-0442(1999)012<2538:IVOTMJ>2.0.CO;2.

Hersbach, H., and Coauthors, 2020: The ERA5 global reanalysis. *Quart. J. Roy. Meteor. Soc.*, **146**, 1999–2049, https://doi.org/10.1002/qj.3803.

Hsu, H.-H., and M.-Y. Lee, 2005: Topographic effects on the eastward propagation and initiation of the Madden–Julian oscillation. *J. Climate*, **18**, 795–809, https://doi.org/10.1175/JCLI-3292.1.

Hsu, P., and T. Li, 2012: Role of the boundary layer moisture asymmetry in causing the eastward propagation of the Madden–Julian oscillation. *J. Climate*, **25**, 4914–4931, https://doi.org/10.1175/JCLI-D-11-00310.1.

Huang, B., and Coauthors, 2017: Extended Reconstructed Sea Surface Temperature, version 5 (ERSSTv5): Upgrades, validations, and intercomparisons. *J. Climate*, **30**, 8179–8205, https://doi.org/10.1175/JCLI-D-16-0836.1.

Inness, P. M., and J. M. Slingo, 2006: The interaction of the Madden–Julian Oscillation with the Maritime Continent in a GCM. *Quart. J. Roy. Meteor. Soc.*, **132**, 1645–1667, https://doi.org/10.1256/qj.05.102.

——, ——, E. Guilyardi, and J. Cole, 2003: Simulation of the Madden–Julian oscillation in a coupled general circulation model. Part II: The role of the basic state. *J. Climate*, **16**, 365–382, https://doi.org/10.1175/1520-0442(2003)016<0365:SOTMJO>2.0.CO;2.

Jiang, X., and Coauthors, 2015: Vertical structure and physical processes of the Madden-Julian oscillation: Exploring key

Brought to you by University of Hawaii at Manoa, Library | Unauthenticated | Downloaded 05/30/23 01:47 AM UTC

model physics in climate simulations. *J. Geophys. Res. Atmos.*, **120**, 4718–4748, https://doi.org/10.1002/2014JD022375.

Johnson, R. H., T. M. Rickenbach, S. A. Rutledge, P. E. Ciesielski, and W. H. Schubert, 1999: Trimodal characteristics of tropical convection. *J. Climate*, **12**, 2397–2418, https://doi.org/10.1175/1520-0442(1999)012<2397:TCOTC>2.0.CO;2.

Kaufman, L., and P. J. Rousseeuw, 2009: *Finding Groups in Data: An Introduction to Cluster Analysis*. John Wiley and Sons, 342 pp.

Kemball-Cook, S. R., and B. C. Weare, 2001: The onset of convection in the Madden–Julian oscillation. *J. Climate*, **14**, 780–793, https://doi.org/10.1175/1520-0442(2001)014<0780:TOOCIT>2.0.CO;2.

Kerns, B. W., and S. S. Chen, 2016: Large-scale precipitation tracking and the MJO over the Maritime Continent and Indo-Pacific warm pool. *J. Geophys. Res. Atmos.*, **121**, 8755–8776, https://doi.org/10.1002/2015JD024661.

Kiladis, G. N., K. H. Straub, and P. T. Haertel, 2005: Zonal and vertical structure of the Madden–Julian oscillation. *J. Atmos. Sci.*, **62**, 2790–2809, https://doi.org/10.1175/JAS3520.1.

Kim, D., J.-S. Kug, and A. H. Sobel, 2014: Propagating versus nonpropagating Madden–Julian oscillation events. *J. Climate*, **27**, 111–125, https://doi.org/10.1175/JCLI-D-13-00084.1.

Kim, H., D. Kim, F. Vitart, V. E. Toma, J. Kug, and P. J. Webster, 2016: MJO propagation across the Maritime Continent in the ECMWF Ensemble Prediction System. *J. Climate*, **29**, 3973–3988, https://doi.org/10.1175/JCLI-D-15-0862.1.

Liebmann, B., and C. A. Smith, 1996: Description of a complete (interpolated) outgoing longwave radiation dataset. *Bull. Amer. Meteor. Soc.*, **77**, 1275–1277, https://doi.org/10.1175/1520-0477-77.6.1274.

Lin, J., B. Mapes, M. Zhang, and M. Newman, 2004: Stratiform precipitation, vertical heating profiles, and the Madden–Julian oscillation. *J. Atmos. Sci.*, **61**, 296–309, https://doi.org/10.1175/1520-0469(2004)061<0296:SPVHPA>2.0.CO;2.

Liu, F., L. Zhou, J. Ling, X. Fu, and G. Huang, 2016: Relationship between SST anomalies and the intensity of intraseasonal variability. *Theor. Appl. Climatol.*, **124**, 847–854, https://doi.org/10.1007/s00704-015-1458-2.

Lyon, B., A. G. Barnston, and D. G. Dewitt, 2014: Tropical Pacific forcing of a 1998–1999 climate shift: Observational analysis and climate model results for the boreal spring season. *Climate Dyn.*, **43**, 893–909, https://doi.org/10.1007/s00382-013-1891-9.

Maloney, E. D., and D. L. Hartmann, 1998: Frictional moisture convergence in a composite life cycle of the Madden–Julian oscillation. *J. Climate*, **11**, 2387–2403, https://doi.org/10.1175/1520-0442(1998)011<2387:FMCIAC>2.0.CO;2.

——, and S.-P. Xie, 2013: Sensitivity of tropical intraseasonal variability to the pattern of climate warming. *J. Adv. Model. Earth Syst.*, **5**, 32–47, https://doi.org/10.1029/2012MS000171.

——, Á. F. Adames, and H. X. Bui, 2019: Madden–Julian oscillation changes under anthropogenic warming. *Nat. Climate Change*, **9**, 26–33, https://doi.org/10.1038/s41558-018-0331-6.

Moon, J.-Y., B. Wang, and K.-J. Ha, 2011: ENSO regulation of MJO teleconnection. *Climate Dyn.*, **37**, 1133–1149, https://doi.org/10.1007/s00382-010-0902-3.

Raghavendra, A., P. E. Roundy, and L. Zhou, 2019: Trends in tropical wave activity from the 1980s to 2016. *J. Climate*, **32**, 1661–1676, https://doi.org/10.1175/JCLI-D-18-0225.1.

Rui, H., and B. Wang, 1990: Development characteristics and dynamic structure of tropical intraseasonal convection anomalies. *J. Atmos. Sci.*, **47**, 357–379, https://doi.org/10.1175/1520-0469(1990)047<0357:DCADSO>2.0.CO;2.

Rushley, S. S., D. Kim, and Á. F. Adames, 2019: Changes in the MJO under greenhouse gas-induced warming in CMIP5 models. *J. Climate*, **32**, 803–821, https://doi.org/10.1175/JCLI-D-18-0437.1.

Seager, R., M. Cane, N. Henderson, D.-E. Lee, R. Abernathey, and H. Zhang, 2019: Strengthening tropical Pacific zonal sea surface temperature gradient consistent with rising greenhouse gases. *Nat. Climate Change*, **9**, 517–522, https://doi.org/10.1038/s41558-019-0505-x.

Slingo, J. M., D. P. Rowell, K. R. Sperber, and F. Nortley, 1999: On the predictability of the interannual behaviour of the Madden-Julian oscillation and its relationship with El Niño. *Quart. J. Roy. Meteor. Soc.*, **125**, 583–609, https://doi.org/10.1256/smsqj.55410.

Sobel, A., S. Wang, and D. Kim, 2014: Moist static energy budget of the MJO during DYNAMO. *J. Atmos. Sci.*, **71**, 4276–4291, https://doi.org/10.1175/JAS-D-14-0052.1.

Sperber, K. R., 2003: Propagation and the vertical structure of the Madden–Julian oscillation. *Mon. Wea. Rev.*, **131**, 3018–3037, https://doi.org/10.1175/1520-0493(2003)131<3018:PATVSO>2.0.CO;2.

Suematsu, T., and H. Miura, 2018: Zonal SST difference as a potential environmental factor supporting the longevity of the Madden–Julian oscillation. *J. Climate*, **31**, 7549–7564, https://doi.org/10.1175/JCLI-D-17-0822.1.

Suhas, E., and B. N. Goswami, 2010: Loss of significance and multidecadal variability of the Madden–Julian oscillation. *J. Climate*, **23**, 3739–3751, https://doi.org/10.1175/2010JCLI3180.1.

Teng, H., and B. Wang, 2003: Interannual variations of the boreal summer intraseasonal oscillation in the Asian–Pacific region. *J. Climate*, **16**, 3572–3584, https://doi.org/10.1175/1520-0442(2003)016<3572:IVOTBS>2.0.CO;2.

Tian, B., D. E. Waliser, E. J. Fetzer, B. H. Lambrigtsen, Y. L. Yung, and B. Wang, 2006: Vertical moist thermodynamic structure and spatial–temporal evolution of the MJO in AIRS observations. *J. Atmos. Sci.*, **63**, 2462–2485, https://doi.org/10.1175/JAS3782.1.

Waliser, D., and Coauthors, 2009: MJO simulation diagnostics. *J. Climate*, **22**, 3006–3030, https://doi.org/10.1175/2008JCLI2731.1.

Wang, B., 1988: Dynamics of tropical low-frequency waves: An analysis of the moist Kelvin wave. *J. Atmos. Sci.*, **45**, 2051–2065, https://doi.org/10.1175/1520-0469(1988)045<2051:DOTLFW>2.0.CO;2.

——, and H. Rui, 1990: Dynamics of the coupled moist Kelvin–Rossby wave on an equatorial $\beta$-plane. *J. Atmos. Sci.*, **47**, 397–413, https://doi.org/10.1175/1520-0469(1990)047<0397:DOTCMK>2.0.CO;2.

——, and X. Xie, 1997: A model for the boreal summer intraseasonal oscillation. *J. Atmos. Sci.*, **54**, 72–86, https://doi.org/10.1175/1520-0469(1997)054<0072:AMFTBS>2.0.CO;2.

——, and G. Chen, 2017: A general theoretical framework for understanding essential dynamics of Madden–Julian oscillation. *Climate Dyn.*, **49**, 2309–2328, https://doi.org/10.1007/s00382-016-3448-1.

——, and S.-S. Lee, 2017: MJO propagation shaped by zonal asymmetric structures: Results from 24 GCM simulations. *J. Climate*, **30**, 7933–7952, https://doi.org/10.1175/JCLI-D-16-0873.1.

Brought to you by University of Hawaii at Manoa, Library | Unauthenticated | Downloaded 05/30/23 01:47 AM UTC

——, J. Liu, H.-J. Kim, P. J. Webster, S.-Y. Yim, and B. Xiang, 2013: Northern Hemisphere summer monsoon intensified by mega-El Niño/Southern Oscillation and Atlantic multidecadal oscillation. *Proc. Natl. Acad. Sci. USA*, **110**, 5347–5352, https://doi.org/10.1073/pnas.1219405110.

——, F. Liu, and G. Chen, 2016: A trio-interaction theory for Madden–Julian oscillation. *Geosci. Lett.*, **3**, 34, https://doi.org/10.1186/s40562-016-0066-z.

——, and Coauthors, 2018: Dynamics-oriented diagnostics for the Madden–Julian oscillation. *J. Climate*, **31**, 3117–3135, https://doi.org/10.1175/JCLI-D-17-0332.1.

——, G. Chen, and F. Liu, 2019: Diversity of the Madden-Julian oscillation. *Sci. Adv.*, **5**, eaax0220, https://doi.org/10.1126/sciadv.aax0220.

Wang, L., T. Li, E. Maloney, and B. Wang, 2017: Fundamental causes of propagating and nonpropagating MJOs in MJOTF/GASS models. *J. Climate*, **30**, 3743–3769, https://doi.org/10.1175/JCLI-D-16-0765.1.

Wang, T., and T. Li, 2021: Factors controlling the diversities of MJO propagation and intensity. *J. Climate*, **34**, 6549–6563, https://doi.org/10.1175/JCLI-D-20-0859.1.

Wheeler, M., and G. N. Kiladis, 1999: Convectively coupled equatorial waves: Analysis of clouds and temperature in the wavenumber–frequency domain. *J. Atmos. Sci.*, **56**, 374–399, https://doi.org/10.1175/1520-0469(1999)056<0374:CCEWAO>2.0.CO;2.

Wu, C.-H., and H.-H. Hsu, 2009: Topographic influence on the MJO in the Maritime Continent. *J. Climate*, **22**, 5433–5448, https://doi.org/10.1175/2009JCLI2825.1.

Xiang, B., and Coauthors, 2022: S2S prediction in GFDL SPEAR: MJO diversity and teleconnections. *Bull. Amer. Meteor. Soc.*, **103**, E463–E484, https://doi.org/10.1175/BAMS-D-21-0124.1.

Xie, P., and P. A. Arkin, 1997: Global precipitation: A 17-year monthly analysis based on gauge observations, satellite estimates, and numerical model outputs. *Bull. Amer. Meteor. Soc.*, **78**, 2539–2558, https://doi.org/10.1175/1520-0477(1997)078<2539:GPAYMA>2.0.CO;2.

Zhang, C., 2005: Madden–Julian Oscillation. *Rev. Geophys.*, **43**, RG2003, https://doi.org/10.1029/2004RG000158.

——, 2013: Madden–Julian oscillation: Bridging weather and climate. *Bull. Amer. Meteor. Soc.*, **94**, 1849–1870, https://doi.org/10.1175/BAMS-D-12-00026.1.

Zhang, L., and W. Han, 2020: Barrier for the eastward propagation of Madden-Julian oscillation over the Maritime Continent: A possible new mechanism. *Geophys. Res. Lett.*, **47**, e2020GL090211, https://doi.org/10.1029/2020GL090211.

Zhang, C., and J. Ling, 2017: Barrier effect of the Indo-Pacific Maritime Continent on the MJO: Perspectives from tracking MJO precipitation. *J. Climate*, **30**, 3439–3459, https://doi.org/10.1175/JCLI-D-16-0614.1.

Brought to you by University of Hawaii at Manoa, Library | Unauthenticated | Downloaded 05/30/23 01:47 AM UTC